Journal of Catalysis 273 (2010) 245–256

Contents lists available at ScienceDirect

Journal of Catalysis

journal homepage: www.elsevier.com/locate/jcat

Thiophene hydrodesulfurization catalysis on supported Ru clusters: Mechanism and site requirements for hydrogenation and desulfurization pathways

Huamin Wang, Enrique Iglesia *

Department of Chemical Engineering, University of California and Chemical Sciences Division, E.O. Lawrence Berkeley National Laboratory, Berkeley, CA 94720, USA

ARTICLE INFO

Article history:
Received 9 April 2010
Revised 27 May 2010
Accepted 28 May 2010
Available online 1 July 2010

Keywords:
Hydrodesulfurization
Thiophene
Ruthenium
Kinetic
Kinetic isotope effects
Cluster size effect

ABSTRACT

Kinetic and isotopic methods were used to probe elementary steps and site requirements for thiophene hydrogenation and desulfurization on Ru metal clusters. Turnover rates for these reactions were unaffected by whether samples were treated in H_2 or H_2S to form metal and sulfide clusters, respectively, before reaction. These data, taken together with the rate and extent of sulfur removal from used samples during contact with H_2, indicate that active structures consist of Ru metal clusters saturated with chemisorbed sulfur at temperatures, pressures, and H_2S levels relevant to hydrodesulfurization catalysis. Turnover rates and isotopic data over a wide range of H_2, H_2S, and thiophene pressures are consistent with elementary steps that include quasi-equilibrated H_2 and H_2S heterolytic dissociation and thiophene binding with η^1(S) or η^4 coordination onto sulfur vacancies. We conclude that hydrogenation proceeds via addition of protons ($H^{\delta+}$, as –S–$H^{\delta+}$ from H_2 or H_2S dissociation) to η^4 thiophene species, while desulfurization involves C–S activation in η^1(S) species aided by $H^{\delta-}$ species formed via H_2 dissociation. Reactant concentrations influence hydrogenation and desulfurization turnover rates to the same extent, suggesting that the involvement of similar active structures, consisting of vacancies on sulfur-covered Ru clusters. Smaller turnover rates and stronger H_2S inhibition on smaller Ru clusters for hydrogenation and desulfurization routes reflect the stronger sulfur binding and the smaller vacancy concentrations on small clusters, which contain exposed atoms with lower average coordination. A preference for η^1(S) over η^4 thiophene species at the higher sulfur coverages that prevail on smaller Ru clusters causes desulfurization and hydrogenation rate ratios to increase with decreasing cluster size. We conclude that hydrogenation and desulfurization routes require similar active sites and that weaker M–S bonds lead to higher concentrations of kinetically-relevant sulfur vacancies. These elementary steps and site requirements are likely to also prevail on metals and sulfides with M–S bond strengths similar or higher than Ru–S, for which vacancy sites are also present as minority species.

1. Introduction

Sulfur is removed from petroleum-derived streams via hydrodesulfurization (HDS) processes using transition metals and their sulfides as catalysts. Higher conversions of organosulfur species without a concomitant increase in H_2 pressures are required to meet increasingly stringent standards for heteroatom content in transportation fuels. The rational design of more effective HDS catalysts will benefit from advances in experimental and theoretical tools to define more precisely the mechanism and site requirements for these reactions [1–5].

Most previous studies have focused on supported Co(Ni)Mo sulfide catalysts, for which reactivity [6–8] and structural [9–11] models, taken together with simulations [12–14], have been used to suggest specific mechanistic roles for two distinct types of active sites. One site is proposed to catalyze direct C–S cleavage through the involvement of sulfur vacancies (coordinatively unsaturated sites, CUS) at edges of lamellar MoS_2 structures [6–14]. The other site catalyzes hydrogenation and hydrogenolysis of C–C and C–S bonds and resides near the edges of MoS_2 terraces [6–14]. The anisotropic structure of MoS_2 presents considerable challenges in defining, characterizing, and measuring these two types of sites [15]; it also encourages the attribution of specific reactivity based on the compelling geometric non-uniformity of its lamellar structure. The nature, structure, and local environment of the proposed active sites and their relation to HDS reactivity remain, however, the subject of considerable debate after decades of significant study.

We examine here the mechanism and site requirements for highly active Ru-based clusters, which exhibit well-defined isotropic structures suitable for structural and functional assessment by experiment and theory. For such systems, the coordination of exposed surface atoms can be placed in the context of the extensive literature about the effects of cluster size and the structure sensitivity in catalytic reactions for isotropic metal clusters [16]. Noble metals (and/or their sulfides) have been reported to be very active

* Corresponding author. Fax: +1 510 642 4778.
E-mail addresses: iglesia@berkeley.edu, iglesia@cchem.berkeley.edu (E. Iglesia).

0021-9517/$ - see front matter © 2010 Elsevier Inc. All rights reserved.
doi:10.1016/j.jcat.2010.05.019

catalysts for desulfurization and hydrogenation of organosulfur compounds [1,2,17–21]. Ru-based catalysts, in particular, are the most active among these metals [18,20,21], but such comparisons and conclusions are seldom underpinned by rigorous measurements of turnover rates or assessments of the state of Ru-based clusters as metals or sulfides during HDS catalysis.

Ru metal and sulfide clusters can be synthesized with a broad range of dispersion and cluster size on several supports, thus allowing systematic assessment of the catalytic consequences of surface coordination [22,23]. It forms isotropic phases with well-defined structure for both metal and sulfide, and these structures are more amenable to structural and functional characterization than dispersed MoS_2 domains. In addition, the latter require specific promoters, such as Ni or Co, whose presence at non-equivalent and uncertain locations within lamellar structures make the assignment of reactivity to specific sites equivocal.

Most previous studies have claimed that RuS_2 pyrite structures (formed by treating Ru compounds with H_2S) are the active phase during HDS [18,23–29] and that coordinatively unsaturated sites at sulfur vacancies act as the specific catalytic sites [25–29]. RuS_2, however, converts to Ru metal in H_2 at typical HDS temperatures (500–700 K) [27,30,31]. Thus, the persistence of RuS_2 structures during typical HDS catalysis seems implausible. The sulfur vacancies proposed as active sites in RuS_2 [25–29] based on spectroscopic evidence are claimed to bind organosulfur species and to dissociate H_2 and H_2S [27,29,32–34], but these elementary steps and their kinetic relevance, as well as the state of clusters as Ru or RuS_2 during catalysis, have remained speculative and even contradictory among parallel studies.

We report here turnover rates, product selectivities, isotopic data, and a sequence of elementary steps consistent with these data for thiophene reactions on Ru clusters with a broad dispersion range (0.15–0.81, corresponding to cluster with 1.2–6.2 nm mean diameter). The catalytic consequences of H_2 or H_2S treatments shown here provide evidence that active sites reside on Ru metal clusters with surfaces nearly saturated with chemisorbed sulfur during HDS catalysis. Kinetic and isotopic data show that S vacancies are involved in quasi-equilibrated thiophene adsorption and in H_2 and H_2S activation, which form adsorbed species required for kinetically-relevant H-assisted C–S bond cleavage and H-addition reactions for thiophene desulfurization and hydrogenation, respectively. HDS turnover rates decrease with increasing Ru dispersion, because of the stronger S-binding on coordinatively unsaturated Ru atoms, which prevail at surfaces of small clusters, and of the concomitant decrease in the concentration of sulfur vacancies present during steady-state HDS catalysis.

2. Experimental

2.1. Catalyst synthesis

Silica (Cab-O-Sil, HS-5, 310 $m^2\,g^{-1}$) was treated in ambient air at 673 K (0.033 K s^{-1}) for 3 h. Ru was deposited on SiO_2 via previously reported protocols [22] by adding to SiO_2 an aqueous solution of $Ru(NH_3)_6Cl_3$ (Aldrich, 98%) and NaOH (EMD Chemicals Inc., CAS No. 1310-73-2; 11.5 pH; 200 $cm^3\,g^{-1}$ SiO_2). After stirring for 1 h (final pH = 11.2), the solids were filtered and washed with doubly deionized water to remove chloride ions. The sample was kept in vacuum at ambient temperature for >24 h and then treated in flowing dry air (Praxair, 99.99%, 1.0 $cm^3\,g^{-1}\,s^{-1}$) to 353 K (0.033 K s^{-1} ramp rate) for 5 h. The Ru contents were 0.1, 0.3, and 1.0 wt.% (Table 1). These samples were then treated at 473–523 K in flowing dry air (Praxair, 99.99%, 1.0 $cm^3\,g^{-1}\,s^{-1}$ (0.033 K s^{-1} ramp rate)) for 2 h to obtain samples with a broad range of Ru dispersion (0.15–0.81).

Table 1
Ru dispersion, average cluster diameter, and thiophene desulfurization and hydrogenation turnover rates on Ru/SiO_2 catalysts.

Ru (wt.%)	Ru dispersion[a]	Cluster diameter[b] (nm)	Thiophene turnover rate [c]	
			Desulfurization	Hydrogenation
0.1	0.81	1.2	0.033	0.011
0.3	0.68	1.4	0.053	0.019
1.0	0.58	1.6	0.089	0.064
1.0	0.42	2.2	0.10	0.067
0.3	0.36	2.6	0.11	0.067
0.3	0.20	4.7	0.11	0.072
1.0	0.15	6.2	0.12	0.081

[a] From H_2-chemisorption.
[b] Calculated from fractional Ru dispersion.
[c] (mol of thiophene)/(mol of surface Ru s), extrapolate to zero residence time and conversion (623 K, 3.0 MPa of H_2, 2.5 kPa of thiophene).

These samples were treated in H_2 or H_2S to prepare clusters of Ru metal (Ru/SiO_2) or Ru sulfide (RuS_x/SiO_2), respectively. Ru/SiO_2 was prepared by treatment in 9% H_2/He (Praxair, 1.67 $cm^3\,g^{-1}\,s^{-1}$) at 673 K (0.033 K s^{-1}) for 2 h and passivation (0.5% O_2/He; Praxair, 0.05 $cm^3\,g^{-1}\,s^{-1}$) at ambient temperature for 6 h. Passivated samples were treated *in situ* in flowing H_2 (Praxair, 99.999%, 50 $cm^3\,g^{-1}\,s^{-1}$) by heating from ambient temperature to 673 K at 0.033 K s^{-1} and holding for 1 h before catalytic measurements. RuS_x/SiO_2 was prepared by *in situ* treatment on flowing 5% H_2S in He (Prxair, certified mixture, 25 $cm^3\,g^{-1}\,s^{-1}$) by heating from ambient temperature to 673 K at 0.033 K s^{-1} and holding for 2 h before catalytic measurements.

2.2. Characterization of composition, dispersion, and structure of Ru-based catalysts

Ru contents were measured by inductively-coupled plasma-optical emission spectroscopy (ICP-OES; Galbraith laboratories). Ru dispersion (fraction of Ru atoms exposed at surfaces) was determined from uptakes of strongly chemisorbed hydrogen at 313 K using a Quantasorb chemisorption analyzer (Quantachrome Corp.). Samples were heated in flowing H_2 (Praxair, 99.999%, 0.83 $cm^3\,g^{-1}\,s^{-1}$) to 673 K at 0.033 K s^{-1} and holding for 1 h. Samples were then evacuated for 1 h at 673 K to remove adsorbed hydrogen and cooled to 313 K. H_2 uptakes were measured as a function of pressure (6–50 kPa) and extrapolated to zero pressure to obtain the amount of strongly chemisorbed hydrogen. This value was used to estimate Ru dispersion using a 1:1 $H:Ru_{surface}$ chemisorption stoichiometry [35]. Mean cluster sizes were estimated from these dispersions by assuming spherical structures and the atomic density in bulk Ru metal (13.65×10^{-3} nm^3) [35]. The cluster size distributions of Ru/SiO_2 and RuS_x/SiO_2 catalyst after HDS catalysis were also measured by transmission electron microscopy (TEM). RuS_x/SiO_2 and Ru/SiO_2 were prepared from the same precursor as described earlier; these samples were used in HDS reactions (623 K, 12 h; 3.0 MPa H_2, 2.5 kPa thiophene) and then treated in H_2S/H_2 mixtures at 623 K for 3 h (3.0 MPa H_2, 3 kPa H_2S, $H_2S/H_2 = 1 \times 10^{-3}$) to simulate conditions prevalent at high thiophene conversions ($H_2S/H_2 = 1–300 \times 10^{-5}$). Samples were then treated in flowing He (Praxair, 99.999%, 10 $cm^3\,g^{-1}\,s^{-1}$), cooled to ambient temperature, and passivated (by contact with flowing 0.5% O_2/He; Praxair, 0.05 $cm^3\,g^{-1}\,s^{-1}$) at ambient temperature for 6 h. Micrographs were obtained using sample powders spread onto a support grid without dispersing them in a liquid using a Philips 420 TEM operated at 120 kV.

The sulfur content in fresh and used RuS_x/SiO_2 samples was determined from the amount of H_2S evolved during temperature-programmed reduction (TPR) using samples with similar Ru amounts (2–4 mg). RuS_x/SiO_2 was prepared as described previously

and RuS_x/SiO_2 and Ru/SiO_2 were also examined after HDS reactions (623 K, 12 h; 3.0 MPa H_2, 2.5 kPa thiophene) and subsequent treatment in H_2S/H_2 mixtures at 623 K for 3 h (3.0 MPa H_2, 3 kPa H_2S, $H_2S/H_2 = 1 \times 10^{-3}$). Samples were then treated in flowing He (Praxair, 99.999%, 10 $cm^3\ g^{-1}\ s^{-1}$) and cooled to ambient temperature. The sulfur content was determined by increasing temperature from ambient to 873 K at 0.167 K s^{-1} and holding for 1 h in a 2% H_2/He stream (8% Ar as reference; 50 $cm^3\ min^{-1}$) while measuring the H_2S concentration in the effluent stream by mass spectrometry (Leybold Inficon, Transpector Series) after calibration with H_2S/H_2/He mixtures of known composition (0.0012, 0.0015, and 0.0020% H_2S). The SiO_2 support did not give any H_2S evolution during H_2 treatment after sulfidation.

The structure of fresh and used RuS_x/SiO_2 samples was probed by X-ray absorption spectroscopy (XAS). Samples were prepared using the same procedure as in TPR measurements. After cooling to ambient temperature in He flow, treated samples were rapidly transferred in N_2 into a XAS cell, which was sealed with Kapton tape and used to obtain X-ray absorption spectra. Ru K-edge XANES (X-ray Absorption Near-Edge Structure) and EXAFS (Extended X-ray Absorption Fine Structure) spectra were measured at the Stanford Synchrotron Research Laboratory (SSRL) using beamline 4-1 and a Si (2 2 0) double-crystal monochromator. The intensities of the incident photon beam, the post-sample transmitted beam, and the transmitted beam after a reference Ru foil were recorded using three Ar-purged ionization chambers. The Ru foil was used to calibrate incident photon energies (22,117 eV absorption edge). EXAFS data were extracted from the raw data as described previously [36] using Athena software [37]. The fitting analysis was performed with Artemis software [36,37] over a 3–10 $Å^{-1}$ k (photoelectron wave number) range and a 1.2–3 Å R (distance between the absorber atom and a scatterer atom) range.

2.3. Catalytic rates and selectivities

Thiophene HDS turnover rates and product selectivities were measured in a continuous flow packed-bed tubular reactor with plug-flow hydrodynamics. Bed temperatures were measured with a K-type thermocouple held within a stainless sheath in contact with the catalyst. Temperatures were within ±0.5 K of the average bed temperature at all axial positions along the catalyst bed. Catalyst powders were diluted with SiO_2 (Cab-O-Sil, HS-5, 310 $m^2\ g^{-1}$) at 9:1 SiO_2/catalyst mass ratio, and the mixture was pressed and sieved to retain 0.125- to 0.18-mm aggregates. A portion of these diluted aggregates (containing 3.0–10.0 mg of original catalyst) was then physically mixed with acid-washed quartz granules of similar particle size (Fluka, acid purified; 1.0 g) to avoid temperature or concentration gradients that can corrupt the intended kinetic origin of measured rates and selectivities and to ensure that bed lengths were sufficiently long for plug-flow hydrodynamics. Varying the extent of dilution within the pellets (1:1 to 9:1 SiO_2/catalyst ratio) or the catalyst bed (165:1 to 650:1 quartz/catalyst ratio) did not influence measured thiophene turnover rates or product selectivities, confirming the absence of transport artifacts in measurements of turnover rates [38,39].

Catalysts were treated in pure H_2 (Praxair, 99.999%, 50 $cm^3\ g^{-1}\ s^{-1}$, from ambient temperature to 673 K, 0.033 K s^{-1}, 1 h hold) or 5% H_2S/He flow (Prxair, certified mixture, 25 $cm^3\ g^{-1}\ s^{-1}$, from ambient temperature to 673 K, 0.033 K s^{-1}, 2 h hold) *in situ* to form Ru/SiO_2 or RuS_x/SiO_2, respectively (as described earlier), before catalytic measurements. After these treatments, the temperature was decreased to 623 K, the pressure of H_2 was increased to desired pressure, and thiophene reactants were introduced using a high-pressure syringe pump (ISCO 500D) and vaporized into the flowing stream. The reactant stream contained thiophene (Alfa Aesar, 99%, 1–10 kPa), n-decane (Sigma–Aldrich, 99+%; 50 kPa, as thiophene solvent and internal standard), and H_2 (Praxair, 99.999%, 1.0–3.0 MPa). Kinetic effects of H_2S were determined by adding a 2% H_2S/H_2 mixture (Praxair, certified mixture) to the reactants to give 2–15 kPa H_2S in the inlet stream. All transfer lines before and after the catalyst bed were kept above 473 K to avoid condensation of reactants or products.

Reactant and product concentrations were measured by on-line gas chromatography (Agilent 6890) using a methyl silicone capillary column (HP-1, Agilent, 25 m × 0.32 mm × 0.52 μm) connected to a flame ionization detector and a Porapak Q packed column (Supelco, 1.82 m × 3.18 mm, 80–100 mesh) connected to a thermal conductivity detector. Blank experiments using SiO_2 did not lead to detectable thiophene conversions. Each sample was allowed to reach steady-state during an initial 15-h stabilization period; rates changed by <5% thereafter over periods of several days.

Turnover rates are reported here as molar thiophene conversion rates per surface Ru atom. Selectivities are reported as the percentage of the converted thiophene appearing as a given product. Residence time (mol surface Ru s mol^{-1} thiophene) is defined as the reciprocal of the space velocity; it was controlled by varying reactant molar rates, while keeping their respective pressures constant. The kinetic response of HDS turnover rates to thiophene, H_2, and H_2S concentration was measured by varying their respective pressures in the inlet stream.

2.4. Kinetic isotopic effects and isotopic exchange rates

Kinetic isotope effects (H_2–D_2, thiophene-d_0/thiophene-d_4) and isotopic exchange rates (H_2–D_2, D_2–H_2S, and D_2–thiophene-d_0) were measured on 1.0 wt.% Ru/SiO_2 (0.58 dispersion) using methods similar to those described in Section 2.3. H_2 and H_2S isotopomers (H_2, HD, D_2, H_2S, DHS, D_2S) were measured by on-line mass spectrometry (Leybold Inficon, Transpector Series). The products of D_2 exchange with thiophene-d_0 were measured by gas chromatography using mass-selective and flame ionization detection (Agilent 6890 GC–MS system). Matrix methods were used to calculate the concentration of thiophene products detected by GC–MS [40]. Thiophene-d_4 (Isotec, chemical purity >99.0%), D_2 (Spectra Gases Inc., UHP), H_2 (Praxair, 99.999%), and H_2S/H_2 (Praxair, certified mixture) were used as reagents. Detailed conditions for each experiment are described together with the corresponding data in the tables and figures included in later sections.

3. Results and discussion

3.1. Catalytic reactions of thiophene on Ru clusters

Rates and selectivities were measured as a function of residence time on Ru/SiO_2 (1 wt.%, 0.58 dispersion) to probe primary and secondary desulfurization pathways. In the absence of added H_2S, thiophene conversion turnover rates decreased with increasing residence time (Fig. 1a). These lower rates reflect the combined kinetic effects of thiophene depletion (3–10% conversion) and inhibition by H_2S products, whose concentration increased with increasing thiophene conversion. The presence of H_2S (10 kPa) in the inlet stream decreased turnover rates and also led to weaker effects of residence time on thiophene turnover rates, because H_2S concentrations changed only slightly with increasing conversion when H_2S was present in the inlet stream. Turnover rates reported hereinafter reflect values extrapolated to zero residence time to exclude any kinetic effects of reactant depletion or inhibition by products and to rigorously reflect the inlet concentrations in the kinetic effects of all species on reaction rates.

Butadiene, 1-butene, *cis*-2-butene, *trans*-2-butene, butane, and tetrahydrothiophene were the only products detected. 1-Butene,

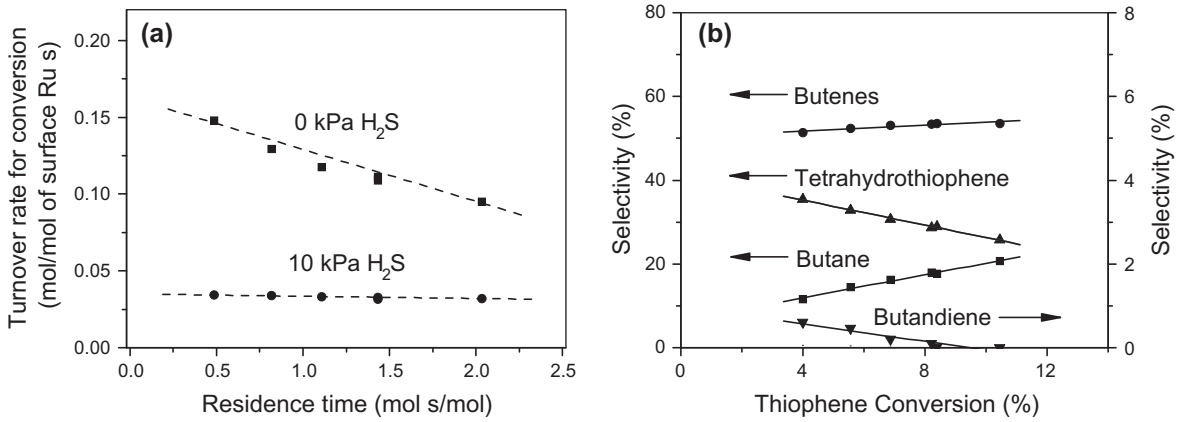

Fig. 1. Total thiophene conversion turnover rates (a) as a function of residence time (the reciprocal of the space velocity) on 1.0 wt.% Ru/SiO_2 (0.58 dispersion) at 623 K, 2.5 kPa C_4H_4S, 3.0 MPa H_2, and 0 kPa (■) or 10 kPa H_2S (●) and product selectivities (b) as a function of thiophene conversion at 0 kPa H_2S.

cis-2-butene, *trans*-2-butene interconversion reactions were equilibrated on all catalysts at all conditions; these products are therefore reported here as a lumped chemical species and denoted as butenes. The non-zero selectivities for butadiene, butenes, and tetrahydrothiophene at low conversions (Fig. 1b) indicate that these species are all primary products, which can form directly from thiophene during one surface sojourn; in contrast, the selectivity trends for *n*-butane indicate that it forms via secondary reactions of primary products. The thiophene to tetrahydrothiophene ratio in the effluent decreased monotonically with increasing residence time, indicating that thiophene and tetrahydrothiophene are not in equilibrium, apparently because hydrogenation–dehydrogenation reactions are too slow to achieve thermodynamic equilibrium. Tetrahydrothiophene selectivities decreased with increasing thiophene conversion, consistent with the subsequent conversion of tetrahydrothiophene to C_4 hydrocarbons via sequential hydrogenation–desulfurization steps. Butadiene selectivities were very low (<10%) and became undetectable above 10% thiophene conversion. *n*-Butane selectivities increased with increasing residence time, because these products represent the thermodynamic endpoint of thiophene conversion pathways at conditions of HDS catalysis. Similar reaction profiles and mechanistic conclusions apply to all Ru catalysts and reaction conditions examined in this study.

These reaction rate and selectivity data are consistent with the sequence of primary and secondary reactions shown in Scheme 1. Thiophene HDS occurs on Ru clusters via parallel pathways involving direct desulfurization (DS) to form butadiene and butenes and hydrogenation (HYD) to form tetrahydrothiophene. Both reactions occur during a single reactive sojourn of thiophene on cluster surfaces. Secondary reactions hydrogenate butadiene and butenes and remove S atoms from tetrahydrothiophene as H_2S. We report here individual DS and HYD turnover rates by separating primary thiophene conversion rates into these two pathways using the initial selectivities measured for tetrahydrothiophene (HYD) and butadiene and butenes (DS pathway) and extrapolated to zero thiophene conversion.

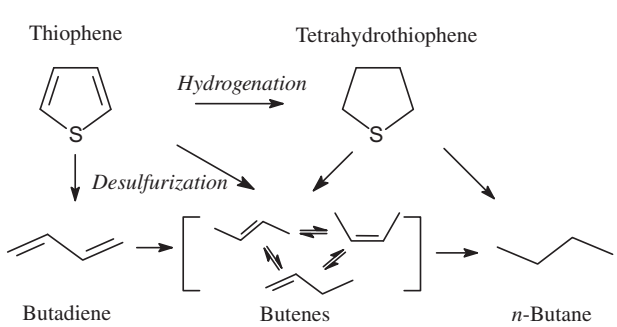

Scheme 1. Proposed reaction network of HDS of thiophene.

3.2. Effects of catalyst treatment on turnover rates and selectivities

Here, we provide experimental evidence for the chemical state of Ru during HDS catalysis by transmission electron micrographs and by comparing HDS turnover rates for catalysts exposed to thiophene–H_2 reactants after treatments that form Ru metal (Ru/SiO_2) or Ru sulfide (RuS_x/SiO_2) clusters. TEM showed that mean cluster diameters ($\langle d \rangle$) were similar after HDS catalysis for 1 wt.% Ru/SiO_2 samples treated in H_2 to form Ru metal clusters ($\langle d \rangle$ = 1.7 nm) or in H_2S to form Ru sulfide clusters ($\langle d \rangle$ = 1.9 nm) (HDS conditions: 2.5 kPa thiophene, 3.0 MPa H_2, 623 K for 12 h, then treated in 3 kPa H_2S, 3.0 MPa H_2, 623 K for 3 h to reproduce typical H_2S/H_2 ratios during HDS, 1×10^{-5} to 3×10^{-3}). Representative TEM images and cluster size distributions are shown in the Supplementary material. These TEM data are consistent with H_2 chemisorption uptakes measured on the fresh sample after H_2 treatment (0.58 dispersion, $\langle d \rangle$ = 1.6 nm), which indicate that Ru species initially present as Ru metal or sulfide preserve their initial dispersion during HDS catalysis and that these dispersions can be rigorously used to estimate turnover rates on both types of samples.

Ru/SiO_2 and RuS_x/SiO_2 samples derived from the same precursor material also gave similar thiophene HDS rates and selectivities, indicating that common active structures were formed during steady-state HDS catalysis irrespective of the initial state of the clusters as either metal or sulfide. Fig. 2 shows that steady-state thiophene DS and HYD turnover rates on Ru/SiO_2 and RuS_x/SiO_2 are identical for any given precursor material. We conclude that the initial oxidation state of Ru (as Ru or RuS_x) is inconsequential for catalytic reactivity in thiophene DS or HYD reactions, apparently because both starting materials form steady-state species with similar structure and composition during steady-state HDS catalysis, irrespective of their different initial state as Ru or RuS_x.

We consider next the chemical state of samples used in HDS catalysis and specifically their sulfur content by measuring the H_2S evolved during their subsequent treatment in H_2. Fig. 3 shows H_2S evolution rates during temperature-programmed treatment in H_2 on RuS_x/SiO_2 (1 wt.%, 0.58 dispersion; treated in 5% H_2S/He 673 K for 2 h; Fig. 3A) before and after thiophene HDS (2.5 kPa thiophene, 3.0 MPa H_2, 623 K for 12 h; then treated in 3 kPa H_2S, 3.0 MPa H_2, 623 K for 3 h, Fig. 3B). Fig. 3C shows similar data on Ru/SiO_2 (0.58 dispersion, treated in H_2 at 673 K for 2 h) used in

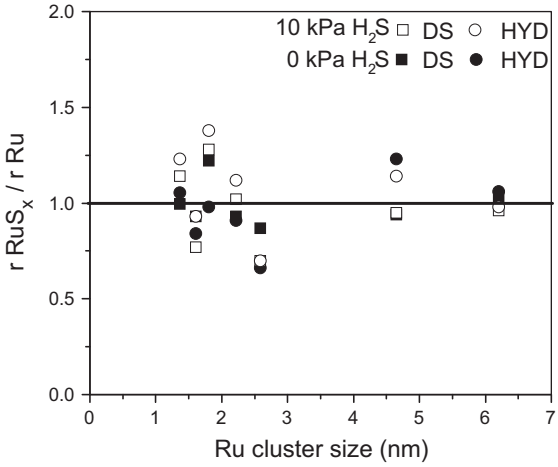

Fig. 2. Effect of pre-treatment on desulfurization and hydrogenation turnover rates of the catalysts with different cluster size. r RuS_x/r Ru represents the ratio of thiophene desulfurization and hydrogenation turnover rates (623 K, 3.0 MPa H_2, 2.5 kPa thiophene, 0 or 10 kPa H_2S) on RuS_x/SiO_2 (pre-treated in H_2S) to those on Ru/SiO_2 (pre-treated in H_2).

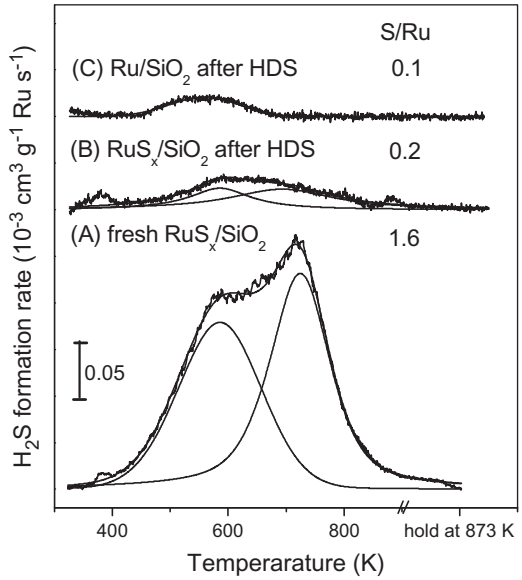

Fig. 3. Temperature-programmed reduction profiles (from ambient to 873 K at 0.167 K s^{-1} and holding for 1 h in a 2% H_2/He stream with a flow rate of 0.0024 cm^3 H_2 g^{-1} Ru metal s^{-1}) of (A) fresh 1 wt.% RuS_x/SiO_2 catalyst, (B) sample (A) used for HDS reaction (3.0 MPa H_2, 3 kPa H_2S, 623 K), and (C) 1 wt.% Ru/SiO_2 catalyst (0.58 dispersion, from the same precursor of (A)) used for HDS reaction.

thiophene HDS at the same conditions as the RuS_x sample in Fig. 3B. Fresh RuS_x/SiO_2 samples showed two H_2S evolution features (at 590 and 723 K) and a S/Ru ratio (1.6) slightly smaller than expected for RuS_2 [23]. After HDS catalysis, the S/Ru ratio decreased to ~0.2 and H_2S evolved from used samples as a broad feature at 600–700 K (Fig. 3B). This feature resembles that in Ru/SiO_2 sample after HDS catalysis (Fig. 3C, S/Ru ~ 0.1). Irrespective of initial treatment and chemical state, the samples used in HDS reactions contain small amounts of sulfur, but these S/Ru ratios are inconsistent with the presence of stoichiometric RuS_2 clusters during HDS catalysis; they indicate instead the presence of chemisorbed sulfur atoms on Ru cluster surfaces. Similar results and conclusions were evident for samples with higher or lower Ru dispersions (0.68, S/Ru = 0.2 after HDS; 0.15, S/Ru = 0.1 after HDS).

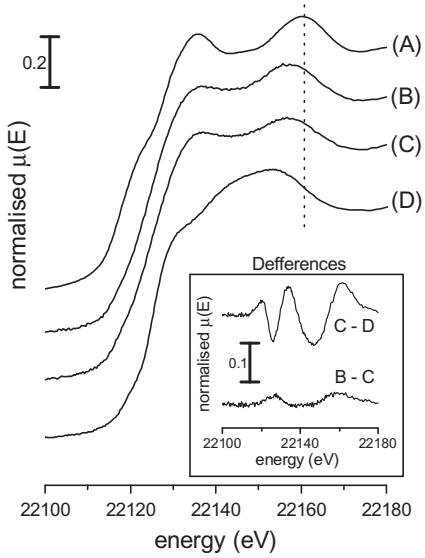

Fig. 4. XANES spectra of (A) Ru foil, (B) 1 wt.% Ru/SiO_2 (0.58 dispersion) catalyst used for HDS reaction (3.0 MPa H_2, 3 kPa H_2S, 623 K), (C) 1 wt.% RuS_x/SiO_2 catalyst (from the same precursor of (B)) used for the HDS reaction (3.0 MPa H_2, 3 kPa H_2S, 623 K), and (D) fresh 1 wt.% RuS_x/SiO_2 catalyst (from the same precursor of (B)). The inset figure shows the differences between the spectra for (C) and (D) and between spectra for (B) and (C).

XAS measurements were performed on Ru/SiO_2 sample (1 wt.%, 0.58, treated in H_2 at 673 K for 2 h) and on RuS_x/SiO_2 (1 wt.%, 0.58 dispersion; treated in 5% H_2S/He 673 K for 2 h) catalysts after thiophene HDS (2.5 kPa thiophene, 3.0 MPa H_2, 623 K for 12 h; then treated in 3 kPa H_2S, 3.0 MPa H_2, 623 K for 3 h). Fig. 4 shows XANES spectra for these samples, Ru foil, and RuS_x/SiO_2. The near-edge spectra of Ru/SiO_2 and RuS_x/SiO_2 samples after HDS are very similar (difference of the two spectra shown in the inset of Fig. 4), suggesting that both starting catalysts form steady-state species with similar structure and composition during steady-state HDS catalysis. The modification of the XANES spectrum of RuS_x/SiO_2 catalyst after use in thiophene HDS is clearly evident from the difference spectra shown in the inset of Fig. 4. XAS spectra of Ru/SiO_2 and RuS_x/SiO_2 after HDS are quite similar to that of Ru foil, but with some features consistent with chemisorbed sulfur. Fig. 5 shows the k^3-weighted radial structure function ($\chi(k)$) for Ru/SiO_2 and RuS_x/SiO_2 after HDS catalysis and for two reference samples (Ru foil and fresh RuS_x/SiO_2). The spectra of fresh RuS_x/SiO_2 resembles that of bulk RuS_2 [36], indicating that sulfidation (673 K, 5% H_2S/He) forms bulk Ru sulfide. The spectra of Ru/SiO_2 and RuS_x/SiO_2 samples after HDS are very similar; one feature corresponds to that for Ru–Ru neighbors in Ru metal and the other one resembles that for Ru–S neighbors in RuS_x/SiO_2. The structural parameters extracted from analysis of these spectra are reported in the Supplementary material. The Ru–Ru coordination number is 7.1–7.8 and that for Ru–S is 2.8–3.5 for these two catalysts after HDS, indicating the structure of Ru species strongly resembling that of Ru metal and the existence of surface sulfidation. These results are similar to those reported for Ru metal clusters treated at 523 K in 2% H_2S/H_2 (8.0 and 2.2 Ru–Ru and Ru–S coordination numbers), a treatment intended to mimic sulfur chemical potentials during HDS catalysts and expected to form metal clusters with saturated sulfur coverages [41].

These turnover rates, taken together with TPR and XAS data, lead us to conclude Ru metal and sulfide clusters form similar structures, consisting of metal clusters saturated with chemisorbed sulfur, during HDS catalysis. This conclusion contradicts previous proposals about the permanence and kinetic relevance of bulk RuS_x

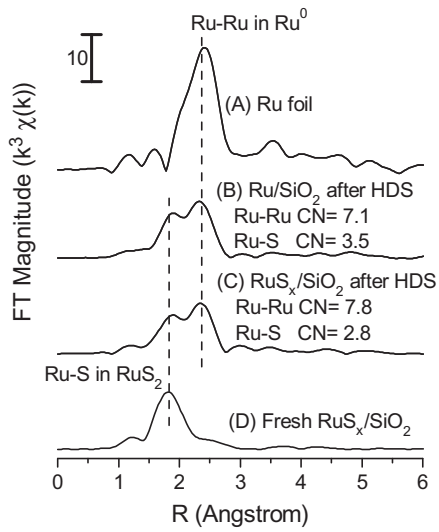

Fig. 5. FT ($k^3\chi(k)$) of the EXAFS spectra of (A) Ru foil, (B) 1 wt.% Ru/SiO_2 (0.58 dispersion) catalyst used for HDS reaction (3.0 MPa H_2, 3 kPa H_2S, 623 K), (C) 1 wt.% RuS_x/SiO_2 catalyst (from the same precursor of (B)) used for the HDS reaction (3.0 MPa H_2, 3 kPa H_2S, 623 K), and (D) fresh 1 wt.% RuS_x/SiO_2 catalyst (from the same precursor of (B)). Some structural parameters (coordination number, CN) from EXAFS for (B) and (C) are also shown.

clusters and about the role of M–S bond energies in the corresponding bulk sulfides in determining the reactivity of HDS catalysts. Our data and conclusions are consistent with the involvement of nearly saturated sulfur coverages at surfaces of Ru clusters with a metallic bulk and with the relevant role of sulfur-binding energies at metal cluster surfaces, instead of bulk sulfides, in controlling their surface reactivity and HDS turnover rates.

These results are consistent with the observed reduction of RuS_x species (formed by reactions of Ru precursors with H_2S) at temperatures and H_2S/H_2 ratios typical of HDS catalysis [27,30,31]. $RuS_2/\gamma\text{-}Al_2O_3$ (prepared at 673 K in 15% H_2S/N_2) reduces during thiophene HDS at 623 K [30] and RuS_2 (prepared at 673 K in 15% H_2S/N_2) dispersed inside Y-zeolites formed Ru metal at 493–593 K [31]. Taken together, our data and these previous studies indicate that the Ru/SiO_2 catalysts contain metal clusters during all kinetic and mechanistic experiments reported below.

3.3. Kinetic effects of reactant and product concentrations on thiophene hydrogenation and desulfurization rates

The detailed effects of thiophene, H_2, and H_2S pressures on DS and HYD turnover rates were measured on two Ru/SiO_2 catalysts (1.0 wt.%, 0.58 dispersion; 0.3 wt.%, 0.36 dispersion) at 623 K. We present here detailed kinetic data for one of these samples (0.58 dispersion; Fig. 6); the results and conclusions were similar on the other catalyst, and the kinetic data on the latter sample are reported in the Supplementary material.

DS and HYD turnover rates increased with increasing H_2 pressure (Fig. 6a; 2.5 kPa thiophene, 0 kPa H_2S). The DS to HYD turnover rate ratios were, however, independent of H_2 pressure. Similar effects of hydrogen are evident from the data in Fig. 6b for experiments in which H_2S was present in the inlet stream ($H_2S/H_2 = 0.005$). DS and HYD turnover rates increased with increasing thiophene pressure (Fig. 6c; 3.0 MPa H_2, 0 kPa H_2S). Their ratio was independent of thiophene pressure, as also observed for the kinetic effects of H_2 pressure. A similar kinetic response to thiophene was observed over a broader range of H_2 and H_2S pressures than that shown in Fig. 6c, and these data are included in the regression analysis of the kinetic data described in Section 3.5. The kinetic effects of thiophene on rates were weaker than for H_2 (Fig. 4a and c), apparently because thiophene-derived intermediates are present at higher coverages than those derived from H_2 during steady-state HDS catalysis and surface coverages of thiophene-derived intermediates approach saturation with increasing thiophene pressures.

H_2S strongly inhibited HDS reactions on metals and sulfides [1,5,19], apparently because sulfur atoms bind strongly on exposed metal atoms or sulfur vacancies, which are required to bind the intermediates involved in kinetically-relevant HDS elementary steps (as discussed in Section 3.5). On Ru/SiO_2, DS turnover rates decreased markedly (0.097–0.0005 mol (mol^{-1} surface Ru) s^{-1}) as inlet H_2S pressures increased (from 0 to 15 kPa; Fig. 6d). The corresponding effects on HYD turnover rates were weaker; as a result, DS to HYD rate ratios decreased from 1.5 to 0.4 with increasing H_2S pressure (from 0 to 15 kPa; Fig. 6d). A stronger H_2S inhibition of DS rates relative to HYD rates was reported also for dibenzothiophene and 4,6-dimethyldibenzothiophene reactions on Mo and NiMo sulfides [42]. These effects have been interpreted as evidence for the involvement of different active sites in DS and HYD pathways. Such an interpretation seems less appropriate for isotropic structures, such as those prevalent on Ru clusters; moreover, it is also awkward in light of the remarkable insensitivity of DS/HYD rate ratios to either H_2 or thiophene pressure, which led us to conclude that DS and HYD turnovers require similar active structures and kinetically-relevant steps. As discussed below (Section 3.5), we propose that these weaker effects of H_2S on HYD (relative to DS) are consistent with the involvement of sulfur vacancies on Ru cluster surfaces as active sites in both reactions; differences in their relative sensitivity to H_2S reflects the involvement of protons formed via H_2S dissociation in HYD but not DS pathways.

The measured kinetic effects of H_2, thiophene, and H_2S pressures for thiophene DS pathways resemble those reported on NiMo sulfides [8] and pre-sulfided Ru [24]; these previous studies did not address the kinetic response of HYD pathways or cover the broad range of relevant H_2, thiophene, and H_2S pressures examined here. We note that HYD pathways ignored in these previous studies are specially relevant as the principal sulfur removal route for larger sterically-hindered organosulfur compounds, such as 4,6-dimethyldibenzothiophene [43].

Next, we report isotopic evidence for the reversibility and kinetic relevance of specific elementary steps (Section 3.4) and show that this sequence of elementary steps accurately describes the measured kinetic effects of H_2, thiophene, and H_2S on thiophene DS and HYD rates (Section 3.5).

3.4. Kinetic isotopic effects and isotopic evidence for reversible H_2 and H_2S dissociation

Kinetic isotope effects (r_H/r_D) were measured from thiophene DS and HYD turnover rates (extrapolated to zero residence time) using H_2–thiophene-d_0, D_2–thiophene-d_0, and D_2–thiophene-d_4 reactants (1.0 and 3.0 MPa of H_2 or D_2, 2.5 and 10 kPa of thiophene) at 623 K on Ru/SiO_2 catalyst (1.0 wt.%); 0.58 dispersion. The measured kinetic isotope effects (KIE) are shown in Table 2. H_2/D_2 kinetic isotope effects near unity (1.0–1.1) were observed for thiophene DS at all conditions tested; these values were only slightly larger (1.2–1.3) for HYD rates. These data may be taken as evidence for kinetically-relevant steps that do not involve H_2-derived species, but such conclusions would be inconsistent with strong effects of H_2 on HYD and DS turnover rates. As discussed in Section 3.5, these weak isotope effects reflect instead compensation effects of equilibrium isotope effects for H_2 dissociation steps and normal kinetic isotope effects for subsequent irreversible and kinetically-relevant steps that use chemisorbed hydrogen. Equilibrium isotope effects for dihydrogen dissociation are typically

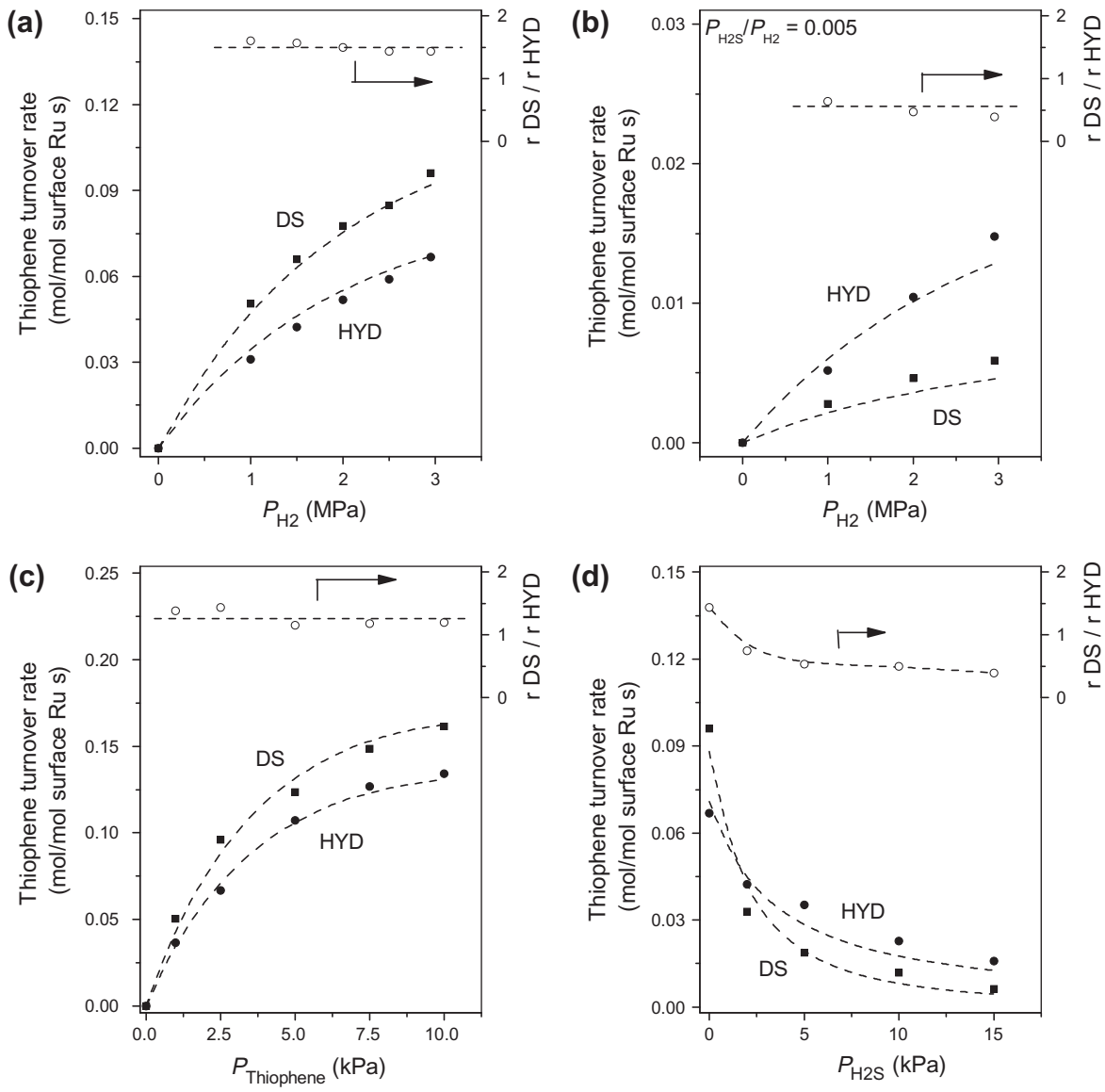

Fig. 6. Effect of H_2 ((a) 2.5 kPa thiophene, 0 kPa H_2S; (b) 2.5 kPa thiophene, a fixed H_2S to H_2 ratio of 0.005), thiophene ((c) 3.0 MPa H_2, 0 kPa H_2S), and H_2S ((d) 3.0 MPa H_2, 2.5 kPa thiophene) pressure on thiophene desulfurization (DS, ■), hydrogenation (HYD, ●) turnover rates and their ratio (○) on 1.0 wt.% Ru/SiO_2 (0.58 dispersion) at 623 K.

Table 2
Kinetic isotope effects for thiophene HDS on 1.0 wt.% Ru/SiO_2 at 623 K and 0 kPa H_2S.

	Pressures		Kinetic isotope effect (r_H/r_D)[a]	
	Thiophene (kPa)	H_2 or D_2 (MPa)	Desulfurization	Hydrogenation
(H_2/D_2)–thiophene	2.5	3.0	1.0	1.2
(H_2/D_2)–thiophene	2.5	1.0	1.1	1.3
D_2–(d_0/d_4 thiophene)	2.5	1.0	1.1	1.0
(H_2/D_2)–thiophene	10.0	1.0	1.1	1.3

[a] Ratio of rates for protium and deuterium forms of hydrogen or thiophene.

smaller than unity because stronger M–D bonds (vs. M–H) offset the larger dissociation energy of D–D bonds (vs. H–H) [44]. Similar compensation effects have been proposed to account for inverse H_2/D_2 isotope effects in methanation [45] and Fischer–Tropsch synthesis [46]. The slightly larger H_2/D_2 KIE value for HYD relative to DS is likely to reflect a larger normal isotope effect for subsequent reactions of H or D atoms in HYD than for hydrogen addition steps in DS pathways as a result of differences in the lateness of the transition states involved in these two otherwise analogous reactions.

The presence of deuterium within thiophene did not lead to detectable kinetic effects (KIE values of 1.1 (DS) and 1.0 (HYD)). The equilibrium constant for molecular adsorption of thiophene is not expected to differ for d_0 and d_4 isotopologues, consistent with these data. These negligible isotope effects also show that subsequent C–H bond activation in adsorbed thiophene, which would have led to normal kinetic isotope effects, is not involved in kinetically-relevant steps required for either DS or HYD reactions. Reversible activation of C–H bonds in thiophene, however, was evident from fast isotopic exchange between D_2 and thiophene-d_0 (H/D exchange rate is 1.5 mol of thiophene/(mol of surface Ru s) higher than that of thiophene chemical conversion (both DS and HYD; 0.14 mol of thiophene/(mol of surface Ru s)) at 2.5 kPa thiophene and 3.0 MPa D_2 on Ru/SiO_2 with 0.58 dispersion), consistent with previous thiophene–D_2 data on MoS_2 at 673 K and ambient pressures [47].

The reversibility of the dihydrogen dissociation steps required by HDS stoichiometry was probed by comparing H_2/D_2 isotopic exchange rates with those for chemical conversion of dihydrogen in

thiophene HDS reactions on Ru/SiO_2 (1.0 wt.%, 0.58 dispersion; 2.5 kPa of thiophene, 3.0 or 1.0 MPa of $H_2 + D_2$, 0 or 5 kPa H_2S). Quasi-equilibrated dihydrogen dissociation steps would form binomial isotopic distributions (50% HD for equimolar H_2/D_2). Mixed isotopomers were detected at 623 K, 1.0 or 3.0 MPa of $H_2 + D_2$, with both 0 and 5 kPa H_2S in the inlet stream. The $H_2/HD/D_2$ ratios were 1:2.0 ± 0.1:1.0 ± 0.1 at all thiophene conversions (0.2–20%) and reaction conditions, consistent with binomial isotopic distributions and with concomitant full equilibration of hydrogen dissociation–recombination steps.

The reversibility of H_2S dissociative adsorption was confirmed from the rate of formation of $H_{2-x}D_xS$ isotopomers during thiophene reactions (2.5 kPa) with equimolar H_2/D_2 mixtures (3.0 or 1.0 MPa) containing H_2S (5 kPa). At both 1.0 and 3.0 MPa pressures, significant amounts of DHS and D_2S were detected; even at low thiophene conversion levels, the $H_2S/DHS/D_2S$ ratios (1:2.1 ± 0.4:1.1 ± 0.3) were those expected from isotopic equilibrium with the prevalent dihydrogen pool (H_2:HD:D_2 = 1:2.0 ± 0.1:1.0 ± 0.1) at all reaction conditions. We conclude that dissociative H_2S adsorption and the recombinative desorption of its chemisorbed fragments are in quasi-equilibrium and also lead to full chemical and isotopic equilibration between H_2 and H_2S during HDS catalysis on Ru metal clusters. As a result, the chemical potential of sulfur during HDS catalysis and the concomitant coverage of chemisorbed sulfur are determined solely by the H_2S/H_2 ratios in the reacting mixture instead of by the individual concentrations of these two molecules.

We conclude that H_2 and H_2S dissociation and the H and SH species that they form remain equilibrated during thiophene HDS on Ru cluster surfaces. As discussed below, H_2S is expected to dissociate heterolytically on vacancy–sulfur site pairs to form two protons (–S–$H^{\delta+}$), while H_2 forms a proton–hydride pair. H–D exchange between H_2 and H_2S becomes possible via recombination of a hydride (from H_2) with a proton (from H_2S). Such chemical equilibration between H_2 and D_2 (and D_2 and H_2S) has been assumed to also occur on Ni(Co)Mo sulfides at lower temperatures and pressures (353 K; 0.2 MPa) than required in HDS practice [48].

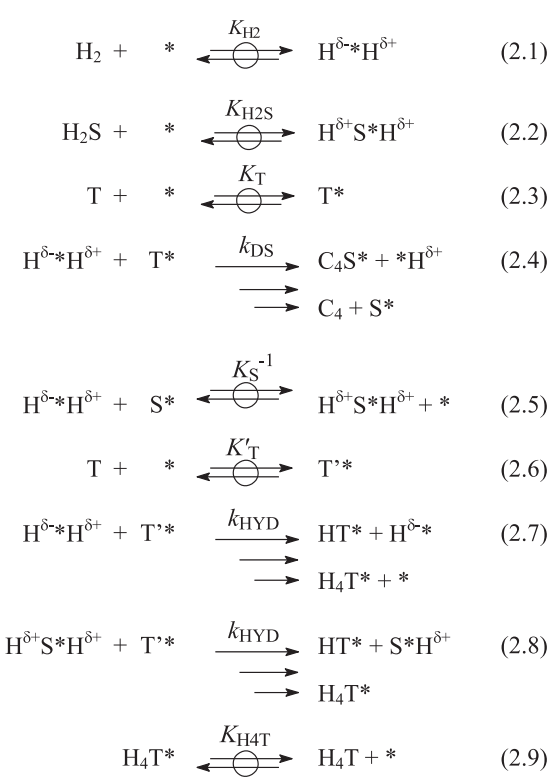

Scheme 2. Proposed reaction pathways for hydrodesulfurization of thiophene on supported Ru metal clusters. (* represents the vacancy–sulfur site pair, #–#S; T, T*, and T'* represent thiophene, η^1(S)-coordinated thiophene, and η^4-coordinated thiophene, respectively; H_4T represents tetrahydrothiophene; k_n and K_n are the kinetic and equilibrium constants, respectively).

3.5. Elementary steps in HDS of thiophene on supported Ru cluster

Here, we combine the kinetic and isotopic data shown above to discuss and define a plausible sequence of elementary steps and their kinetic relevance, as well as the reactive species involved and their surface coverages, during thiophene–H_2 reactions on Ru clusters. These elementary steps are shown in Scheme 2, in which * represents a vacancy–sulfur anion site pair (#–#S, # is a vacancy exposing a Ru surface atom, as shown in Scheme 1), ⇌ denotes a quasi-equilibrated step, and k and K are the kinetic and equilibrium constants, respectively, for each elementary steps.

Active sites consisting of vicinal sulfur vacancies and sulfur anions have been claimed to be involved in HDS catalysis on metal sulfides [1,25]. The surface concentration of these site pairs during catalysis depends on temperature and H_2S/H_2 ratios, as well as on the identity and structure of the catalytic structures within which they reside. Thiophene and H_2S can adsorb competitively on such site pairs, which have been invoked to interpret rate data for thiophene HDS on sulfided CoMo catalyst [49], arene hydrogenation in the presence of H_2S on Mo sulfides [50–52], and 2-methylthiophene HDS and olefin hydrogenation on a series of transition metal sulfides [53,54]. Here, we consider the involvement of site pairs consisting of a vacancy (#) and a sulfur anion (#–S^{2-}) in thiophene DS and HYD reactions on Ru metal surfaces (Scheme 1). These surfaces are nearly saturated with chemisorbed sulfur species, as expected from the strong binding sulfur atoms on Ru surfaces [55].

The sulfur chemical potential and surface coverage depend on H_2S/H_2 ratios according to the thermodynamics of the reaction:

$$\mathrm{Ru} + \mathrm{H_2S} \leftrightarrow \mathrm{Ru{-}S(surface)} + \mathrm{H_2}, \Delta G^0_{ads} = RT\ln(P_{H_2S}/P_{H_2}) \quad (1)$$

ΔG^0_{ads} was estimated from enthalpies and entropies on Ru/Al_2O_3 (1.5 wt.%, 0.34 dispersion) at sulfur coverages near unity (θ_S = 1.00 ± 0.16; where θ_S represents the fractional coverage based on Ru dispersion values) [56]. ΔG^0_{ads} is −64 kJ mol^{-1} (623 K), corresponding to H_2S/H_2 ratios of $\sim 4 \times 10^{-6}$ to give saturation sulfur coverages. These H_2S/H_2 ratios are significantly smaller than those prevalent during HDS reactions in our study ($10–3000 \times 10^{-6}$), suggesting that surfaces are indeed nearly saturated with sulfur during steady-state HDS catalysis. Therefore, vacancy–sulfur site pairs, required for thiophene binding and H_2 and H_2S activation and for kinetically-relevant steps in HYD and DS reactions, exist as minority surface species. H_2S inhibition of DS and HYD reactions is consistent with the involvement of sulfur vacancies in kinetically-relevant steps. Scheme 3 depicts vacancies as electron-withdrawing centers (Lewis acid) and sulfur anions (–S^{2-}) as proton-abstracting sites (Brønsted base) that form SH groups with significant Brønsted acid character. The presence of Lewis and Brønsted acid sites on metal sulfides has been inferred from infrared spectra of CH_3SH adsorbed on RuS_x [27,29] and H_2S adsorbed on MoS_2 [34].

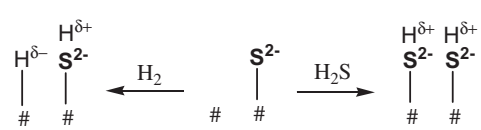

Scheme 3. Proposed mechanisms of the dissociation of H_2 and H_2S on the vacancy–sulfur site pair (#–#S).

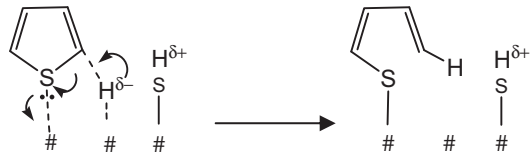

Scheme 4. Proposed mechanism of the cleavage of the first C–S bond of η^1(S)-coordinated thiophene.

Scheme 5. Proposed mechanism of the addition of the first hydrogen to η^4-coordinated thiophene.

Our isotopic data show that H_2 dissociation (step 2.1, Scheme 3) is quasi-equilibrated; this step can proceed via heterolytic routes to form $H^{\delta-}$ and $H^{\delta+}$ (as –S–$H^{\delta+}$) on surfaces nearly saturated with chemisorbed sulfur atoms. $H^{\delta+}$ and –S–$H^{\delta+}$ species have been detected by neutron scattering [31,32] and ^{1}H NMR [33] during H_2 adsorption on substoichiometric RuS_{2-x}. Our isotopic data show that H_2S dissociation is also equilibrated during thiophene HDS reactions on Ru clusters. The heterolytic dissociation of H_2S to form –S–$H^{\delta+}$ (on vacancies) and $H^{\delta+}$ (on sulfur anions; as –S–$H^{\delta+}$ (step 2.2, Scheme 3)) is consistent with the formation of thiolate species on vacancies and SH groups on sulfur anions from CH_3SH (the methyl homolog of H_2S) on RuS_2 [27,29]. Recombination and desorption of H_2 (steps 2.1, 2.2 and 2.5) after H_2S dissociation can then form chemisorbed sulfur atoms.

Organometallic analogs and theoretical treatments suggest that thiophene can adsorb on sulfur vacancies in η^1(S), η^1(C), η^2(C = C), η^4 η^5, and η^4-S-μ_2 configurations [1,12]. Thiophene adsorbs on exposed Ni in substoichiometric NiS_x clusters via η^1(S)- and η^4-coordination (Scheme 4 and Scheme 5, respectively); η^4 structures are favored on surfaces with lower sulfur content, while η^1(S) structures prevail at higher sulfur coverages [12]. We propose here similar adsorption modes (steps 2.3 and 2.6), with binding onto sulfur vacancies via σ-bonds with the lone pair in S atoms (η^1(S), T* in step 2.3 of Scheme 2; Scheme 4) and π-bonding via the aromatic ring (η^4; T′* in step 2.6 of Scheme 2; Scheme 5). We suggest also that thiophene adsorbed in η^1(S)-coordination favors desulfurization, and η^4-species favor hydrogenation based on the stronger effects of Ru cluster size on HYD than on DS pathways discussed below (Section 3.6).

The subsequent reactions of $H^{\delta-}$ or –S–$H^{\delta+}$ species with adsorbed thiophene are irreversible and kinetically-relevant (steps 2.4, 2.7, 2.8). For DS pathways, Scheme 4 shows this reaction as the cleavage of the first C–S bond in thiophene (step 2.4). The C–S bond in η^1(S)-coordinated thiophene reacts with vicinal $H^{\delta-}$ to form an adsorbed thiolate, which rapidly cleaves the remaining C–S bond to form butadiene or its hydrogenated derivatives during one or more surface sojourns. The remaining S atoms react with hydrogen to form H_2S (step 2.5). H and SH species have been invoked without consensus about their specific role in HDS reactions in many previous mechanistic proposals [1,6,25,49,53,54]. In our proposed mechanism, $H^{\delta-}$ is involved in attack at the carbon adjacent to the sulfur atom in thiophene, while the lone pair in the sulfur atom interacts with a sulfur vacancy (Lewis acid site). These concerted steps weaken the C–S bond and form stable thiolate intermediates (Scheme 4).

Scheme 5 depicts –S–$H^{\delta+}$ reactions with η^4-thiophene to form protonated species as the first step in thiophene HYD pathways (steps 2.7, 2.8); a subsequent $H^{\delta-}$ attack then completes a hydrogenation turnover. The initial dihydrothiophene product was observed in trace amounts (<0.2% selectivity) on Ru catalysts at low thiophene conversions (<5%); it undergoes rapid hydrogenation either during one surface sojourn as it forms or after desorption and subsequent readsorption onto another site. Dihydrothiophene is present, however, at much higher concentrations as a reactive intermediate during thiophene HDS on Pt-based catalysts [57]. The attack of unsaturated species by protons has been implicated in the hydrogenation of arenes on MoS_2 [50–52,58] and in the hydrogenation of thiophene on CoMo sulfides [49]. With H_2S/H_2 mixtures, $H^{\delta+}$ species can form via heterolytic dissociation of either H_2 (step 2.1) or H_2S (step 2.2). As a result, HYD routes can use a source of protons (from H_2S) unavailable in DS pathways and HYD reactions are found to be less sensitive to H_2S inhibition than parallel DS reactions (Fig. 6d).

The elementary steps in Scheme 2 and the pseudo steady-state assumption for all intermediates lead to closed-form equations for turnover rates of DS (Eq. (2)) and HYD (Eq. (3)) reactions:

$$r_{DS} = \frac{k_{DS} K_T P_T K_{H_2} P_{H_2}}{\alpha^2} \tag{2}$$

$$r_{HYD} = \frac{k_{HYD}(K_{H_2} P_{H_2} + K_{H_2S} P_{H_2S}) K'_T P_T}{\alpha^2} \tag{3}$$

in terms of H_2, thiophene, and H_2S pressures and of the rate or equilibrium constants for the relevant elementary steps. The derivation is shown in detail in the Supplementary material. Each term in the common denominator of these equations represents the concentration of one of the intermediates involved relative to the corresponding concentration of sulfur vacancies; this denominator is denoted as α in Eqs. (2) and (3) and defined as:

$$\alpha = \underset{*}{1} + \underset{T^*}{K_T P_T} + \underset{T'^*}{K'_T P_T} + \underset{H^*H}{K_{H_2} P_{H_2}} + \underset{HS^*H}{K_{H_2S} P_{H_2S}} + \underset{S^*}{K_S \frac{K_{H_2S} P_{H_2S}}{K_{H_2} P_{H_2}}} \tag{4}$$

where the species noted under each term defines its relation to a specific surface intermediate. A term containing H_2S pressures appears in the numerator of the rate equation for HYD but not for DS, causing HYD/DS ratios to increase with H_2S pressure while

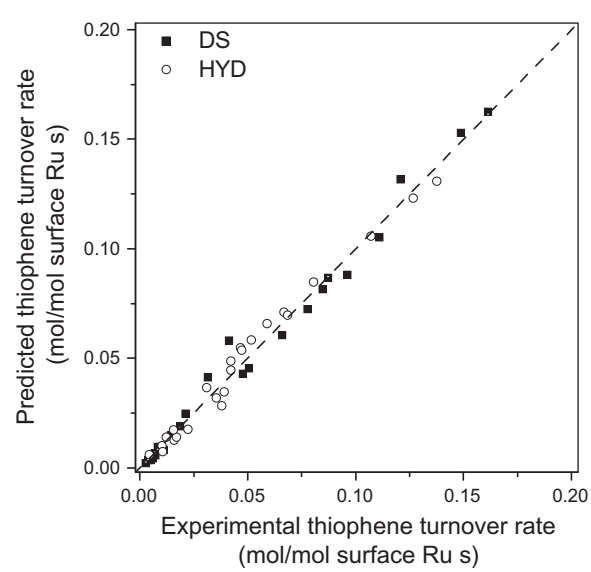

Fig. 7. Parity plots for the predicted (from Eqs. (2) and (3) and kinetic parameters in Table 3 for 1.6 nm Ru/SiO_2 catalyst) and measured thiophene desulfurization (■) and hydrogenation (○) turnover rates at 623 K.

Table 3
Kinetic parameters estimated for thiophene HDS on Ru/SiO_2 at 623 K.

Kinetic parameters[a]	Ru cluster diameter (nm)		Ratio[b]
	1.6	2.6	
$K_T k_{DS}$ (kPa^{-1} mol/mol s)	0.23 (±0.06)	0.31 (±0.09)	1.4
$K'_T k_{HYD}$ (kPa^{-1} mol/mol s)	0.18 (±0.07)	0.22 (±0.07)	1.3
$K_T + K'_T$ (kPa^{-1})	0.11 (±0.02)	0.16 (±0.04)	1.5
K_{H2} (kPa^{-1})	$1.7 (\pm 0.9) \times 10^{-4}$	$1.7 (\pm 1.1) \times 10^{-4}$	1.0
K_{H_2S} (kPa^{-1})	$8.9 (\pm 3.6) \times 10^{-2}$	0.11 (±0.04)	1.2
K_S	1.9 (±0.8)	1.0 (±0.3)	0.5

[a] For constants in Scheme 2 and Eqs. (2)–(4).
[b] Ratio of constant for 2.6 nm catalyst to that for 1.6 nm catalyst.

remaining insensitive H_2 or thiophene pressures for a given H_2S pressure, consistent with kinetic results.

Fig. 7 shows that Eqs. (2) and (3) accurately describe measured thiophene DS and HYD turnover rates over a 30-fold range in turnover rates. Rate and equilibrium constants derived by the regression analysis for Ru/SiO_2 (0.58 dispersion, 1.6 nm clusters) are reported in Table 3. The sensitivity analysis shown in the Supplementary material indicates that best value of these parameters lies within relatively sharp error minima in the regression analysis and that measured rates are strongly sensitive to the values of these parameters. Equilibrium constants for thiophene and H_2S are much larger than for H_2 as expected from the strong binding of sulfur-containing compounds, specially H_2S, also reported on MoS_2 and $NiMoS_x$ catalysts [1,8]. The relative values of these equilibrium constants show S* species are much more abundant than HS*H at the conditions of these experiments; they also demonstrate that inhibition by H_2S reflects predominantly the titration of vacancies by S* and depends on H_2S/H_2 ratios and not independently on H_2 or H_2S pressures. Larger Ru clusters on SiO_2 (2.6 nm; 0.36 dispersion) gave identical rate equations and excellent agreement with rate data (Supplementary material); their kinetic parameters for HYD and DS routes are also shown in Table 3 and will be discussed in the context of the catalytic consequences of cluster size in the next section.

In the context of these rate equations, measured H_2/D_2 kinetic isotope effects for DS and HYD rates reflect the ratios of Eqs. (2) and (3), respectively, for H_2 and D_2 co-reactants:

$$KIE_{DS} = \frac{r_{DS,H}}{r_{DS,D}} = \frac{k_{DS,H}K_{H_2}}{k_{DS,D}K_{D_2}} \times \beta \quad (5)$$

$$KIE_{HYD} = \frac{r_{HYD,H}}{r_{HYD,D}} = \frac{k_{HYD,H}K_{H_2}}{k_{HYD,D}K_{D_2}} \times \beta \quad (6)$$

$$\beta = \left(\frac{1 + K_T P_T + K'_T P_T + K_{D_2} P_{D_2}}{1 + K_T P_T + K'_T P_T + K_{H_2} P_{H_2}}\right)^2 \quad (7)$$

which contain isotope effects of both equilibrium (K_{H2}/K_{D2}) and kinetic ($k_{DS,H}/k_{DS,D}$ or $k_{HYD,H}/k_{HYD,D}$) origins. Dissociative H_2 adsorption typically gives inverse isotope effects because D* binds significantly more strongly than H* on metals [44–46,59]. Density functional theory estimates give smaller equilibrium constants for dissociative chemisorptions of H_2 than D_2 (by ~0.7 at 500 K) on Fe surfaces [60]. H_2/D_2 mixtures lead to inverse equilibrium isotope effects (0.4–0.7 at 300–350 K) on organometallic complexes [44]. Assuming a tentative value of 0.7 for dihydrogen dissociation equilibrium isotope effect (K_{H2}/K_{D2}) on Ru, Eqs. (5)–(7) and the constants in Table 3 lead to normal H_2/D_2 kinetic isotopic effects for the kinetically-relevant surface reactions in both DS and HYD pathways ($k_{DS,H}/k_{DS,D}$ = 1.2–1.4, step 2.4; $k_{HYD,H}/k_{HYD,D}$ = 1.4–1.8, step 2.7; details on the calculation are shown in Supplementary material). These small normal isotope effects are consistent with a role of hydrogen-derived species in the C–S bond cleavage and hydrogen addition reactions that control DS and HYD rates, respectively, and with reactant-like transition states proposed in Schemes 4 and 5 for DS and HYD, respectively.

The catalytic sequence proposed in Scheme 2 requires only one type of site, consisting of sulfur vacancies on nearly saturated surfaces of Ru metal clusters, for the elementary steps involved in thiophene DS and HYD routes. We consider that DS and HYD involve specific roles of $H^{\delta-}$ (for DS) and –S–$H^{\delta+}$ (for HYD) species, and we use these concepts here to accurately describe kinetic and isotopic effects on these two desulfurization pathways. In contrast, most previous studies have assigned different structures and locations to the active sites required for DS and HYD pathways. It is plausible that layered MoS_2 structures expose different sites and that they are independently involved in these two HDS pathways. We conclude, however, from the evidence herein provided that such disparate structures are not inherently required to catalyze HYD and DS routes, because isotropic Ru clusters, without the brim or edge sites of layered MoS_2 structures [6–14], catalyze both desulfurization routes using similar active sites for both reactions. We find it unnecessary to propose different sites for HYD and DS routes and would, in any case, be unable to make any such proposals consistent with the isotropic nature of Ru metal clusters. These conclusions are also relevant to other metals and even to Co and Ni structures supported on MoS_2 species in bimetallic catalysts. Some recent studies have also proposed the involvement of similar site pairs in thiophene HDS and alkene hydrogenation on bulk mono- and bimetallic sulfides [54,61]. We extend these concepts next by interpreting the effects of Ru cluster size on HYD and DS turnover rates using these proposals for the elementary steps and the sites required for these reactions.

3.6. Effects of Ru cluster size on thiophene HYD and DS turnover rates

The size of metal clusters causes significant changes in the relative exposure of atoms with different coordination at surfaces. Specifically, coordination decreases with decreasing size for clusters smaller than 10 nm as corners and edges become more abundant relative to low-index terrace planes [16,62]. Surface atoms with lower coordination tend to bind intermediates more strongly because of their greater coordinative unsaturation, thus causing the coverage of such species to increase as clusters become smaller. Next, we examine and interpret HYD and DS turnover rates on Ru clusters prepared on SiO_2 with a broad range of dispersion (0.15–0.81 dispersion, 1.2–6.2 nm cluster diameter). In this study, we have varied the size of Ru clusters by changing the Ru content (0.1–1.0 wt.%) and the temperatures (353–523 K) at which these samples were treated in flowing dry air before reduction and use in HDS catalysis.

Thiophene DS and HYD turnover rates with 0 or 10 kPa H_2S present in the inlet stream are shown for Ru clusters of different size in Fig. 8 and Table 1. Thiophene DS and HYD turnover rates (at both 0 and 10 kPa H_2S) increased markedly with increasing Ru cluster size (1.2–2.6 nm) initially and then more gradually for larger clusters (2.6–6.2 nm) (Fig. 6a and b). These trends suggest that the low-index planes exposed on surfaces of larger clusters are more effective at catalyzing the kinetically-relevant steps for both HYD and DS pathways and that their relative abundance increases with size until such low-index planed become the predominant species for clusters larger than ~10 nm. These trends appear to reflect, at least in part, the expected weaker binding of sulfur on more coordinatively-saturated surface atoms at low-index planes and the concomitantly higher concentrations of sulfur vacancies with increasing Ru cluster size.

The effects of Ru cluster size on the ratio of the reaction rates at 0 and 10 kPa H_2S reflect the relative sensitivity to inhibition of DS and HYD routes by chemisorbed sulfur species, the surface coverage of which decreases with increasing cluster size (Fig. 8c). H_2S

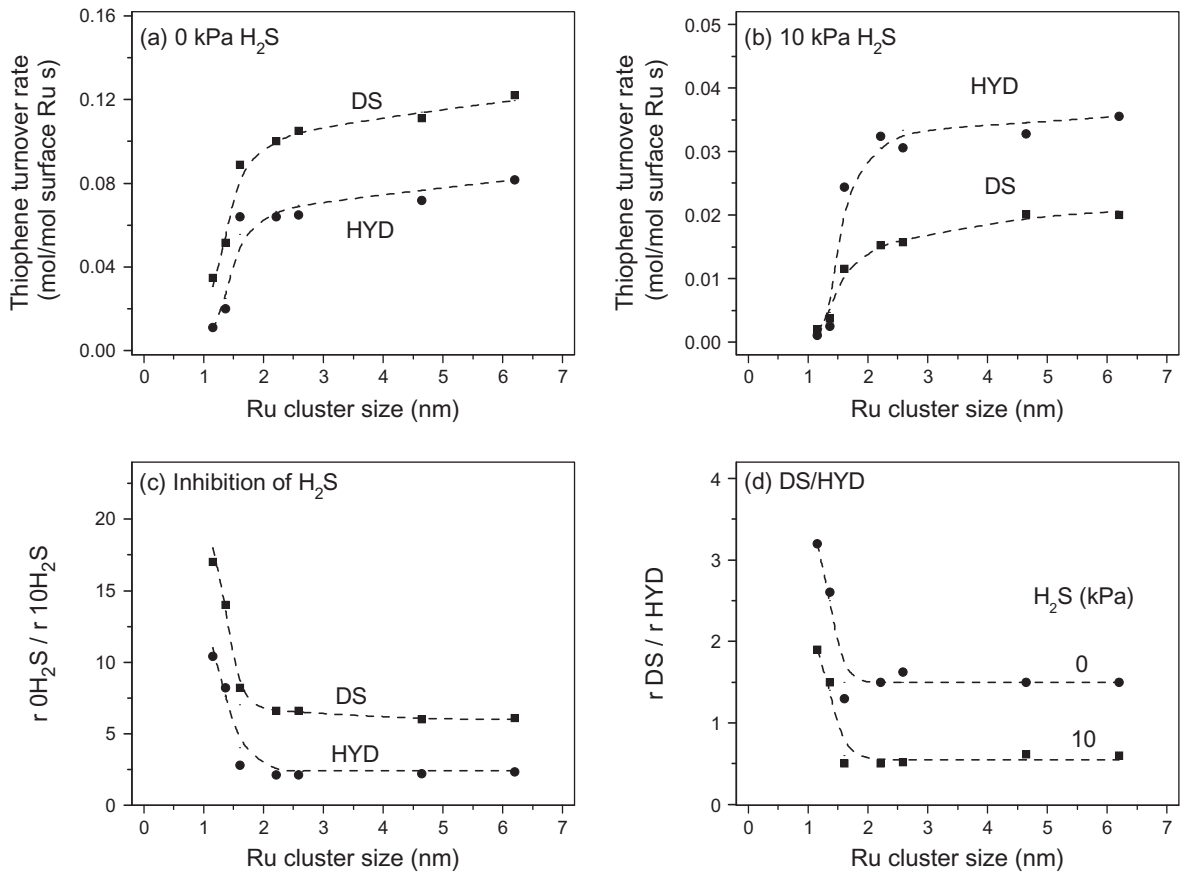

Fig. 8. Thiophene desulfurization and hydrogenation turnover rates ((a) at 0 kPa H_2S; (b) at 10 kPa H_2S), inhibition degree of H_2S (ratio of turnover rates for DS and HYD at 0 kPa H_2S to those at 10 kPa H_2S (c)), and pathway selectivity (ratio of turnover rates for desulfurization and hydrogenation (d)) over Ru/SiO_2 catalyst with different cluster size (623 K, 3.0 MPa H_2, 2.5 kPa thiophene, 0 or 10 kPa H_2S).

inhibition effects on both DS and HYD reactions are much stronger on smaller than on larger clusters, indicating a stronger binding of sulfur on smaller clusters. The ratio of reaction rates at both 0 and 10 kPa H_2S remained unchanged for clusters larger than 2.6 nm (Fig. 8c), as also found for the turnover rates for the individual HYD and DS routes (Fig. 8a and b). Table 3 shows that the equilibrium constant (K_S) for H_2S dissociation to form sulfur anions (steps 2.1, 2.2, 2.5) is larger on the smaller clusters, because coordinatively unsaturated surface Ru atoms, which bind sulfur more strongly, are more abundant on such small clusters. As a result, turnover rates decrease as metal clusters become smaller, because of a concomitant decrease in the concentration of sulfur vacancies. The size of Ru clusters influences the number of sulfur anion-vacancy site pairs available for dissociation of H_2 and H_2S and for thiophene adsorption; these steps are required to form the adsorbed species involved in the kinetically-relevant steps for DS and HYD reactions. We note that, according to the volcano curve concept [53,54,63], weaker M–S bond in bulk transition metal sulfides would improve their activity, relevant with our conclusion here in bulk metallic Ru with sulfur-covered surface. However, one should be noted that such heteroatom bonds at metal surfaces are typically much stronger than in the corresponding bulk compound.

The effects of Ru cluster size on the ratio of DS to HYD rates reflect their relative sensitivity to the coordinative unsaturation of exposed atoms. Fig. 8d shows that DS and HYD turnover rates depend differently on Ru cluster size. The ratio of DS to HYD turnover rates increased with decreasing Ru cluster size, indicating that the binding energy of sulfur, which is higher on smaller clusters, influences HYD routes more strongly than DS pathways, in spite of their similar site requirements. We suggest that smaller clusters, with their higher sulfur coverages, favor η^1(S)-coordination (Scheme 4) instead of the η^4-coordination (Scheme 5), which has been shown to be favored at lower coverages. As a result, DS pathways, via η^1(S)-coordinated thiophene, prevail on smaller clusters, consistent with the reported preference for η^1(S) over η^4 coordination on vacancies on NiS_x clusters as the sulfur coverage increases [12].

The effects of Ru cluster size predominantly reflect the concomitant effects of sulfur-binding strength on the equilibrium concentration of sulfur vacancies and the involvement of such vacancies in kinetically-relevant steps for both DS and HYD reactions. This conclusion is consistent with the elementary steps in Scheme 2 and with the rate equation derived from this Scheme and supported by our rate and isotopic data. Similar effects of metal cluster size on turnover rates have been reported for dimethyl ether combustion [64], methane combustion [65], and NO oxidation [66] on supported Pt clusters and for methane oxidation on supported PdO_x clusters [67]; these reactions share a common requirement for kinetically-relevant steps on site pairs involving a vacancy site on surfaces nearly saturated with heteroatoms (S or O). In all cases, such vacancies become increasingly scarce as the binding strength of these heteroatoms increases with the coordinative unsaturation brought forth by a decrease in cluster size.

4. Conclusions

Kinetic and isotopic measurements provide a consistent mechanistic picture of thiophene hydrodesulfurization turnovers on supported Ru clusters. This reaction occurs via two parallel pathways: desulfurization to butadiene and butenes and hydrogenation

to tetrahydrothiophene, both involving kinetically-relevant steps; both reactions occur on site pairs consisting of an adsorbed sulfur atom and a vacancy site on Ru surfaces. Thiophene adsorbs on sulfur vacancies via η^1(S)- or η^4-coordination and H_2 and H_2S are heterolytically dissociated on site pairs via quasi-equilibrated steps, consistent with the effects of reactants and products on rates and with isotopic evidence. Subsequently, the formed adsorbed species perform H-assisted C–S bond cleavage of η^1(S)-thiophene or hydrogen addition reaction of η^4-thiophene that control thiophene desulfurization and hydrogenation rates, respectively. The rate equation derived from the proposed sequence of elementary steps is consistent with the kinetic response of thiophene desulfurization and hydrogenation turnover rates to thiophene, H_2, and H_2S concentrations. Temperature-programmed reduction, transmission electron microscopy, and turnover rate measurements indicate that pre-treatment of the catalyst in H_2 or H_2S at 673 K (form Ru or RuS_x, respectively) does not affect the structure and composition of Ru clusters during hydrodesulfurization at 623 K and H_2S/H_2 ratio range of 1×10^{-5} to 3×10^{-3}, which remain metallic, but surfaces are nearly saturated with chemisorbed sulfur, consistent with the involvement of nearly saturated sulfur coverages at surfaces of Ru clusters with a metallic bulk in controlling their surface reactivity and hydrodesulfurization turnover rates. Both thiophene desulfurization and hydrogenation turnover rates are lower on small Ru clusters, which also show stronger H_2S inhibitory effects and lower selectivities to hydrogenation. These size effects reflect that smaller clusters, with more coordinatively unsaturated surface atoms, bind sulfur more strongly than larger clusters and exhibit higher steady-state sulfur coverage, which lead to lower vacancy concentrations and more preferable η^1(S) thiophene adsorption than η^4 on smaller clusters. We expect that our conclusions are also relevant to other metals and even to Co and Ni structures supported on MoS_2 species in bimetallic catalysts that require sulfur vacancies for hydrodesulfurization catalysis.

Acknowledgments

This work was supported by the Director, Office of Basic Energy Sciences, Chemical Sciences Division of the US Department of Energy under Contract DE-AC02-05CH11231. X-ray absorption data were collected at Stanford Synchrotron Radiation Laboratory (SSRL), a facility operated by the United States Department of Energy (DOE), Office of Basic Energy Sciences. The authors acknowledge Ms. Cathy Chin and Mr. Brian Weiss of the University of California at Berkeley for helpful technical discussions and for their careful review of this manuscript.

Appendix A. Supplementary material

Supplementary data associated with this article can be found, in the online version, at doi:10.1016/j.jcat.2010.05.019.

References

[1] H. Topsøe, B.S. Clausen, F.E. Massoth, in: J.R. Anderson, M. Boudart (Eds.), Catalysis Science and Technology, vol. 11, Springer-Verlag, New York, 1996, p. 1.
[2] R.R. Chianelli, M. Daage, M.J. Ledoux, Adv. Catal. 40 (1994) 177.
[3] D.D. Whitehurst, T. Isoda, I. Mochida, Adv. Catal. 42 (1998) 345.
[4] M.J. Girgis, B.C. Gates, Ind. Eng. Chem. Res. 30 (1991) 2021.
[5] R. Prins, V.H.J. de Beer, G.A. Somorjai, Catal. Rev. Sci. Eng. 31 (1989) 1.
[6] S. Kasztelan, D. Guillaume, Ind. Eng. Chem. Res. 33 (1994) 203.
[7] V. Vanrysselberghe, G.F. Froment, Ind. Eng. Chem. Res. 35 (1996) 3311.
[8] A. Borgna, E.J.M. Hensen, J.A.R. can Veen, J.W. Niemantsverdriet, J. Catal. 221 (2004) 541.
[9] S. Helveg, J.V. Lauritsen, E. Lægsgaard, I. Stensgaard, J.K. Nørskov, B.S. Clausen, H. Topsøe, F. Besenbacher, Phys. Rev. Lett. 84 (2000) 951.
[10] J.V. Lauritsen, J. Kibsgaard, G.H. Olesen, P.G. Moses, B. Hinnemann, S. Helveg, J.K. Nørskov, B.S. Clausen, H. Topsøe, E. Lægsgaard, F. Besenbacher, J. Catal. 249 (2007) 220.
[11] M. Brorson, A. Carlsson, H. Topsøe, Catal. Today 123 (2007) 31.
[12] M. Neurock, R.A. van Santen, J. Am. Chem. Soc. 116 (1994) 4427.
[13] T. Todorova, R. Prins, T. Weber, J. Catal. 236 (2005) 190.
[14] P.G. Moses, B. Hinnemann, H. Topsøe, J.K. Nørskov, J. Catal. 248 (2007) 188.
[15] E.J.M. Hensen, P.J. Kooyman, T. van der Meer, A.M. van der Kraan, V.H.J. de Beer, J.A.R. van Veen, R.A. van Santen, J. Catal. 199 (2001) 224.
[16] M. Boudart, Adv. Catal. 20 (1969) 153.
[17] T.A. Pecoraro, R.R. Chianelli, J. Catal. 67 (1981) 430.
[18] M. Lacroix, N. Boutarfa, C. Guillard, M. Vrinat, M. Breysse, J. Catal. 120 (1989) 473.
[19] A. Niquille-Röthlisberger, R. Prins, J. Catal. 242 (2006) 207.
[20] S. Harris, R.R. Chianelli, J. Catal. 86 (1984) 400.
[21] E.J.M. Hensen, H.J.A. Brans, G.M.H.J. Lardinois, V.H.J. de Beer, J.A.R. van Veen, R.A. van Santen, J. Catal. 192 (2000) 98.
[22] L. Jiao, J.R. Regalbuto, J. Catal. 260 (2008) 329.
[23] P. Castillo-Villalon, J. Ramirez, F. Mauge, J. Catal. 260 (2008) 65.
[24] Y.-J. Kuo, B.J. Tatarchuk, J. Catal. 112 (1988) 229.
[25] M. Breysse, E. Furimsky, S. Kasztelan, M. Lacroix, G. Perot, Catal. Rev. 44 (2002) 651.
[26] J.A.D.L. Reyes, Appl. Catal. A 322 (2007) 106.
[27] G. Berhault, M. Lacroix, M. Breysse, F. Maugé, J.-C. Lavalley, L. Qu, J. Catal. 170 (1997) 37.
[28] A. Ishihara, H. Godo, R. Kanamori, W. Qian, T. Kabe, Appl. Catal. A 182 (1999) 345.
[29] G. Berhault, M. Lacroix, M. Breysse, F. Maugé, J.-C. Lavalley, H. Nie, L. Qu, J. Catal. 178 (1998) 555.
[30] P. Castillo-Villalon, J. Ramirez, R. Cuevas, R. Contreras, R. Luna, H. Vaca, F. Murrieta, Catal. Today 107–108 (2005) 913.
[31] C. Dumonteil, M. Lacroix, C. Geantet, H. Jobic, M. Breysse, J. Catal. 187 (1999) 464.
[32] W.H. Heise, K. Lu, U.-J. Kuo, T.J. Udovic, J.J. Rush, B.J. Tatarchuk, J. Phys. Chem. 92 (1988) 5184.
[33] H. Jobic, G. Clugnet, M. Lacroix, S. Yuan, C. Mirodatos, M. Breysse, J. Am. Chem. Soc. 115 (1993) 3654.
[34] N.-Y. Topsøe, H. Topsøe, J. Catal. 139 (1993) 641.
[35] X. Shen, L.-J. Garces, Y. Ding, K. Laubernds, R.P. Zerger, M. Aindow, E.J. Neth, S.L. Suib, Appl. Catal. A 335 (2008) 187.
[36] J. Blanchard, K.K. Bando, T. Matsui, M. Harada, M. Breysse, Y. Yoshmura, Appl. Catal. A 322 (2007) 98.
[37] B. Ravel, J. Synchrotron Radiat. 12 (2005) 537.
[38] R.M. Koros, E.J. Nowak, Chem. Eng. Sci. 22 (1967) 470.
[39] R.J. Madon, M. Boudart, Ind. Eng. Chem. Fundam. 21 (1982) 438.
[40] G.L. Price, E. Iglesia, Ind. Eng. Chem. 28 (1989) 839.
[41] J. Blanchard, K.K. Bando, M. Breysse, C. Geantet, M. lacroix, Y. Yoshmura, Catal. Today 147 (2009) 255.
[42] H. Wang, R. Prins, J. Catal. 264 (2009) 31.
[43] R. Prins, M. Egorova, A. Röthlisberger, Y. Zhao, N. Sivasankar, P. Kukula, Catal. Today 111 (2006) 84.
[44] R.M. Bullock, B.R. Bender, Isotope methods – homogeneous, in: I.T. Horváth (Ed.), Encyclopedia of Catalysis, Wiley-Interscience, Hoboken, NJ, 2003.
[45] J.L. Costa, A.F. Noels, A. Demonceau, A.J. Hubert, J. Catal. 105 (1987) 1.
[46] S. Krishnamoorthy, M. Tu, M.P. Ojeda, D. Pinna, E. Iglesia, J. Catal. 211 (2002) 422.
[47] K.F. McCarty, G.L. Schrader, J. Catal. 103 (1987) 261.
[48] C. Thomas, L. Viviier, J.L. Lemberton, S. Kasztenlan, G. Pérot, J. Catal. 167 (1997) 1.
[49] J. Leglise, L. Finot, J.N.M. van Gestel, J.C. Duchet, Stud. Surf. Sci. Catal. 127 (1999) 51.
[50] S. Kasztelan, D. Guillaume, Ing. Eng. Chem. Res. 33 (1994) 203.
[51] C.M. Romero, J.W. Thybaut, G.B. Marin, Catal. Today 130 (2008) 231.
[52] S. Blanchin, P. Galtier, S. Kasztelan, S. Kressmann, H. Penet, G. Pérot, J. Phys. Chem. A 105 (2001) 10860.
[53] A. Daudin, S. Brunt, G. Perot, P. Raybaud, C. Bouchy, J. Catal. 248 (2007) 111.
[54] A. Daudin, A.F. Lamic, G. Perot, S. Brunet, P. Raybaud, C. Bouchy, Catal. Today 130 (2008) 221.
[55] C.H. Bartholomew, P.K. Agrawal, J.R. Katzer, Adv. Catal. 31 (1982) 135.
[56] J.G. MaCarty, H. Wise, J. Chem. Phys. 74 (1981) 5877.
[57] H. Wang, E. Iglesia, unpublished results.
[58] L.J. Simon, J.G. van Ommen, A. Jentys, J.A. Lercher, J. Catal. 203 (2001) 434.
[59] G. Welder, F.J. Broker, G. Fisch, G. Schroll, Z. Phys. Chem. Neue Folge 76 (1971) 212.
[60] M. Ojeda, A. Li, E. Iglesia, unpublished results.
[61] N. Dos Santos, H. Dulot, N. Marchal, M. Vrinat, Appl. Catal. A 352 (2009) 114.
[62] R. van Hardeveld, F. Hartog, Surf. Sci. 15 (1969) 189.
[63] H. Toulhoat, P. Raybaud, J. Catal. 216 (2003) 63.
[64] A. Ishikawa, M. Neurock, E. Iglesia, J. Am. Chem. Soc. 129 (2007) 13201.
[65] C. Chin, E. Eglesia, unpublished results.
[66] B.M. Weiss, E. Iglesia, J. Phys. Chem. C 113 (2009) 13331.
[67] K. Fujimoto, F.H. Ribeiro, M. Avalos-Borja, E. Iglesia, J. Catal. 179 (1998) 431.